Direct Observation of Enhanced Raman Scattering on Nano-Sized ZrO$_2$ Substrate: Charge-Transfer Contribution

Peng Ji[1,2], Zhe Wang[2], Xiaohong Shang[1], Yu Zhang[2], Yikuan Liu[2], Zhu Mao[1] and Xiumin Shi[2]*

[1] School of Chemistry and Life Science, Changchun University of Technology, Changchun, China, [2] College of Chemical Engineering, Changchun University of Technology, Changchun, China

Direct observation of the surface-enhanced Raman scattering (SERS) of molecules adsorbed on nano-sized zirconia (ZrO$_2$) substrates was first reported without the need for the addition of metal particles. It was found that ZrO$_2$ nanoparticles can exhibit unprecedented Raman signal enhancements on the order of 10^3 for the probe molecule 4-mercaptobenzoic acid (4-MBA). The dramatic effect of the calcination temperature on the ZrO$_2$ nanoparticles was also investigated. The ZrO$_2$ nanoparticles with the particle diameter of 10.5 nm, which were prepared by calcination at a temperature of 500°C, have the highest SERS activity. A comparison between the experimental and calculation results indicates that charge transfer (CT) effects dominate the surface enhancement. The plentiful surface state of ZrO$_2$ active substrate that is beneficial to CT resonance occurs between molecules and ZrO$_2$ to produce a SERS effect. The CT process depends, to a large extent, on the intrinsic properties of the modifying molecules and the surface properties of the ZrO$_2$. This is a new SERS phenomenon for ZrO$_2$ that will expand the application of ZrO$_2$ to microanalysis and is beneficial for studying the basic properties of both ZrO$_2$ and SERS.

Keywords: raman, SERS, ZrO$_2$, charge-transfer, nanoparticle

INTRODUCTION

The large surface-enhanced Raman scattering (SERS) enhancement observed in metals and semiconductors is explained by the vibrational coupling of various resonances in the molecules of the semiconductor system, such as surface plasmons, excitons, charge transfer (CT), and molecular resonance (Yin et al., 2010; Li et al., 2011; Wang and Chen, 2011; Jiang et al., 2013; Wang et al., 2013, 2014, 2016; Huang et al., 2014; Kadkhodazadeh et al., 2014; Mogensen and Kneipp, 2014; Shiohara et al., 2014; Zhao et al., 2014; Shen et al., 2015; Scott and Carron, 2016; Fu et al., 2019). Because semiconductor materials are widely used in the rapidly developing energy and optoelectronic fields, it is important to investigate the SERS mechanism for semiconductor substrates (Lombardi and Birke, 2014; Alessandri and Lombardi, 2016; Han et al., 2017). Semiconductors that can be used as SERS substrates have been identified, such as TiO$_2$, ZnO, and CdS. These can amplify the Raman signals of surface-adsorbed organic molecules such as 4-mercaptopyridine (4-MPY) and 4-mercaptobenzoic acid (4-MBA) by more than 100-fold (Sun et al., 2007; Wang et al., 2007; Yang et al., 2008).

Nano-sized zirconium dioxide (ZrO$_2$) is one of the most important materials for the preparation of nano-ceramics, and it can prepare ceramic components with various functions (Li et al., 2017). It has applications and developments in solid oxide fuel cells, thermal barrier coating materials, catalyst carriers, lubricant additives, medical, gas sensitive, and wear resistant materials (Duan et al., 2017; Gan et al., 2017; Long et al., 2017; Xu et al., 2017; Wang et al., 2019). The brittleness of ceramic materials limits its practical application, and nanoceramics are a strategic way to solve the brittleness of ceramics. However, grain size is the most important factor affecting the performance of nano-ceramics. The decrease of grain size will significantly improve the mechanical properties of materials (Zhang L. et al., 2015). The grain refinement will contribute to the slip between the grains, giving the material plastic behavior. A large number of studies by researchers have shown that the temperature is closely related to the size of ZrO$_2$ particles, and the transition temperature of ZrO$_2$ particles below 100 nm can be greatly reduced (Becker et al., 2008). Toughening of ceramics by microcracks and residual stresses generated the conversion of ZrO$_2$ from a tetragonal phase (t-ZrO$_2$) to a monoclinic phase (m-ZrO$_2$). Therefore, the nano-sized ZrO$_2$ can significantly increase the strength and stress intensity factor of the ceramic, thereby increasing the toughness of the ceramic (De Aza et al., 2002). Nowadays, the application research on nano-sized ZrO$_2$ has become one of the research hotspots of nano-ceramic new technology. As a new type of high-performance ceramics, the use of highly sensitive SERS technology with *in-situ* characterization advantages to study the size effect of nano-sized ZrO$_2$ is expected to promote the better performance of nano-ceramic materials to enable the emergence of new properties and functions.

In addition, ZrO$_2$ is a particularly attractive candidate to promote CT enhancement because it has recently been shown that the luminescence effect of ZrO$_2$ materials is derived from transitions between new and ground state energy levels formed by oxygen vacancies that capture electrons and oxygen vacancies produced by the formed association center (Kralik et al., 1998; Chang and Doong, 2007). Owing to the photoelectric properties of ZrO$_2$, a CT state is readily formed. Currently, there are no reports on the use of ZrO$_2$ enhancement to obtain SERS (**Figure 1**).

MATERIALS AND METHODS

Chemicals

Zirconium nitrate pentahydrate was obtained from Tianjin Guangfu Fine Chemical Research Institute; triethylamine was obtained from XiLong Chemical Co., Ltd.; CTAB were obtained from China Huishi Biochemical Reagent Co., Ltd. 4-Mercaptobenzoic acid (4-MBA), 4-Mercaptopyridine (4-Mpy), and P-aminothiophenol (PATP) were purchased from Sigma-Aldrich. The other chemicals are analytically pure without further purification.

Synthesis of ZrO$_2$ Nanoparticles

The synthesis of ZrO$_2$ was followed the procedure below (Zhou et al., 2006). First, at room temperature and in a 500 mL round-bottomed flask, mix and dissolve 17.44 g Zirconium Nitrate and 2.95 g Hexadecyl trimethyl ammonium Bromide in 180 mL deionized water. The hydrolysis was carried out with slight stirring. Stirring was continued for about 20 min until a clear sol was obtained. 22.615 mL Triethylamine was added in the solution under rough stirring. The mixture was kept at 75°C for 8 h in the round-bottomed flask. The sol-gel production was dried at 82°C for 48 h. This was the last step after drying the product, eluted with ethanol for 48 h in a Soxhlet extraction. The product was calcined in a muffle furnace for 2 h to obtain ZrO$_2$ nanoparticles at different temperatures (450–650°C).

Adsorption of Probing Molecules

The surface modification of ZrO$_2$ nanocrystals is obtained as follows: 10 mL 4-MBA ethanol solution concentration 1×10^{-3} M was used to dissolve 20 mg of ZrO$_2$ nanocrystals. The mixture was stirred at room temperature for 4 h and then centrifuged. The 4-MBA molecules that did not adsorb were subsequently removed by rinsing the precipitate with absolute deionized water and ethanol once more. ZrO$_2$ Nanoparticles that modify by 4-MBA and PATP are similar to 4-MBA.

Sample Characterization

The crystal structure of the ZrO$_2$ sample was determined by X-ray diffraction using a Rikagu Smartlab X-ray powder diffractometer with 0.15406 nm. The electronic absorption spectra were recorded on a Cary5000 UV-vis spectrophotometer. Raman spectra were obtained with Horiba HR Evolution Raman spectroscopy. The 532 nm radiation from an air-cooled argon ion laser was used as the exciting source. The morphology of ZrO$_2$ nanoparticles was characterized by the JEM-2000EX TEM instrument. A Thermofisher Escalab 250XI X-ray photoelectron spectroscopy (XPS) was applied to investigate the elemental composition and the surface electronic valence state for UPS.

RESULTS AND DISCUSSION

ZrO$_2$ Phonon Modes (XRD & Raman)

Zirconia has three low-pressure structural phases. With increasing temperatures, zirconia changes from a monoclinic phase (m-ZrO$_2$) to a tetragonal phase (t-ZrO$_2$), eventually becoming a cubic phase (Zheng et al., 2009). The monoclinic phase (space group C5 2h or P21/c) is thermodynamically stable at temperatures of <1400 K. At around 1400 K, the t-ZrO$_2$ transition (space group D15 4h or P42/nmc) is stable until 2570 K, and is a slightly distorted form of the cubic structure (Heuer et al., 1982). In this study, the size of the ZrO$_2$ nanoparticles was controlled by adjusting the calcination temperature to change the surface defect state of the nanoparticles to obtain a stronger SERS signal of the surface substance. This is verified by UV-vis spectra of ZrO$_2$ nanoparticles with different calcination temperature, see **Figure S1**.
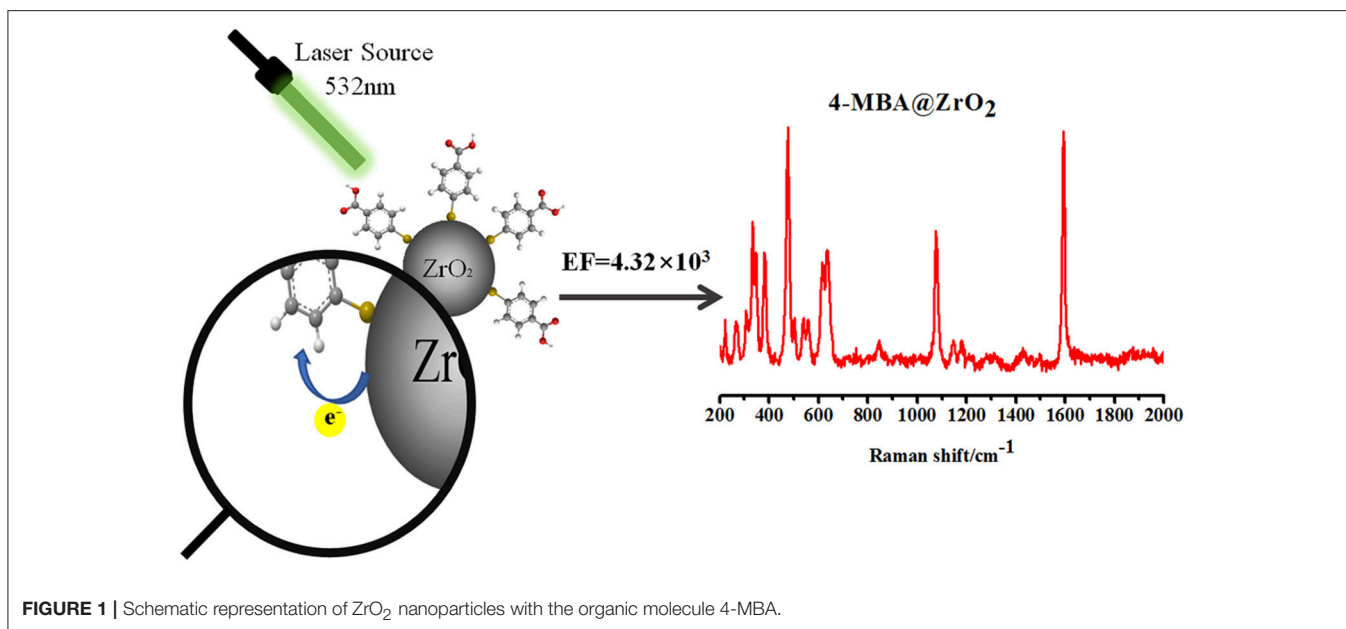
FIGURE 1 | Schematic representation of ZrO$_2$ nanoparticles with the organic molecule 4-MBA.

Increase in Nanoparticle Size With Increasing Calcination Temperature

Figure 2A shows the XRD patterns of ZrO$_2$ nanoparticles calcined at different temperatures. The m-ZrO$_2$ is the dominant phase in these ZrO$_2$ nanoparticles. Almost all of the diffraction peaks are comparable to the standard data and are remarkably sharp, indicating the purity and high crystallinity of the synthesized ZrO$_2$ material. It can be observed that as the calcination temperature increases from 450 to 650°C, the XRD pattern becomes narrower and the sample crystallinity increases. The diameters of the ZrO$_2$ nanoparticles calcined at 450, 500, 550, 600, and 650°C were calculated from the full width at half-maximum using the Scherrer equation. The calculated diameters of the zirconia nanoparticles were 8.1, 10.5, 11.1, 15.5, and 17.6 nm, respectively. Thus, it can be seen that the grain size increases with increasing calcination temperature. The wide XRD peak is attributed to a very small particle size, which is also demonstrated by the transmission electron microscopy (TEM) results (**Figure S2**). As the calcination temperature increases from 450 to 650°C, both of the crystallinity and grain size of the ZrO$_2$ sample gradually increases. As shown in **Figure S3**, the XRD patterns show that the ZrO$_2$ nanoparticles calcined at 500°C primarily exhibit m-ZrO$_2$ (PDF card: 13-307), and there is extremely little t-ZrO$_2$ present (PDF card: 88-1007).

Nanoparticles Primarily Exist in the m-Phase

ZrO$_2$ samples were prepared through the sol-gel method and characterized using Raman spectroscopy (**Figure 2B**). The Raman shift characteristics reflect the energy level change in the specific vibration of the molecules. Tetragonal zirconia has six active vibrational modes (see Equation 1): B1g, Eg, B1g, Eg, A1g, and Eg (Zhao and Vanderbilt, 2002). Monoclinic zirconia has 18 Raman-active vibrational modes

(see Equation 2).

$$\Gamma_{vib}{}^t = A1g + 2B1g + 3Eg \tag{1}$$
$$\Gamma_{vib}{}^m = 9Ag + 9Bg \tag{2}$$

From the Raman spectra and scattering data (see **Figure 2B**), it can be seen that the composition of the synthesized ZrO$_2$ is a mixture of t-ZrO$_2$ and m-ZrO$_2$, with a greater proportion of monoclinic phase. Comparing the Raman spectra, it is observed that the prepared ZrO$_2$ nanoparticles had an Eg vibrational mode at 265 cm^{-1} corresponding to the tetragonal phase. The remaining peaks occurred at 221 cm^{-1} (Bg), 309 cm^{-1} (Bg), 332 cm^{-1} (Bg), 345 cm^{-1} (Ag), 380 cm^{-1} (Ag), 476 cm^{-1} (Ag), 503 cm^{-1} (Bg), 539 cm^{-1} (Bg), 558 cm^{-1} (Ag), 613 cm^{-1} (Bg), and 635 cm^{-1} (Ag) are the vibration modes of m-ZrO$_2$ (Carlone, 1992). **Figure 2B** shows that the 11 active vibrational modes correspond well with the monoclinic phase. This indicates that m-ZrO$_2$ is dominant and the crystallization is relatively good. This point is consistent with the results observed using XRD; however, compared to the XRD patterns, the Raman spectra can reflect the difference in the crystallinity of ZrO$_2$ caused by different calcination temperatures with greater sensitivity.

Size-Dependent of SERS

ZrO$_2$ is an n-type semiconductor, and thus the surface of ZrO$_2$ nanoparticles are rich in oxygen vacancy defects (Navio et al., 2001). To study the effect of the calcination temperature of ZrO$_2$ on the SERS enhancement, SERS spectra of 4-MBA adsorbed on ZrO$_2$ nanoparticles calcined at different temperatures were obtained, as shown in **Figure 3**. The Raman spectra obtained for ZrO$_2$ nanoparticles at varying calcination temperatures can be used to explore the role of surface defects on the CT mechanism. For calcination temperatures in excess of 500°C, as the zirconia
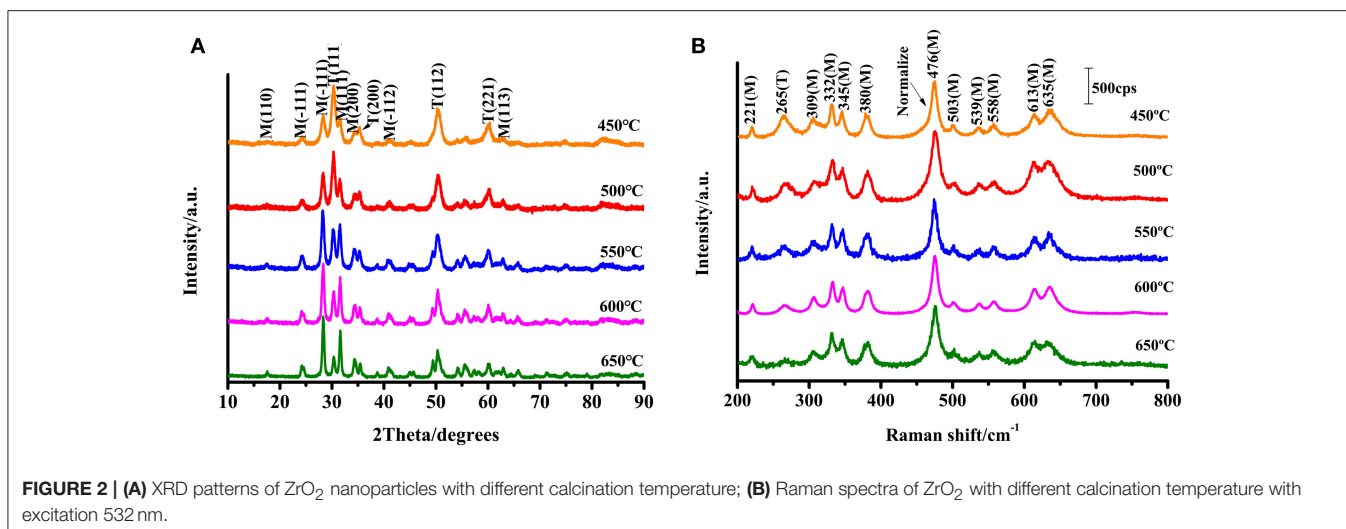
FIGURE 2 | (A) XRD patterns of ZrO$_2$ nanoparticles with different calcination temperature; (B) Raman spectra of ZrO$_2$ with different calcination temperature with excitation 532 nm.
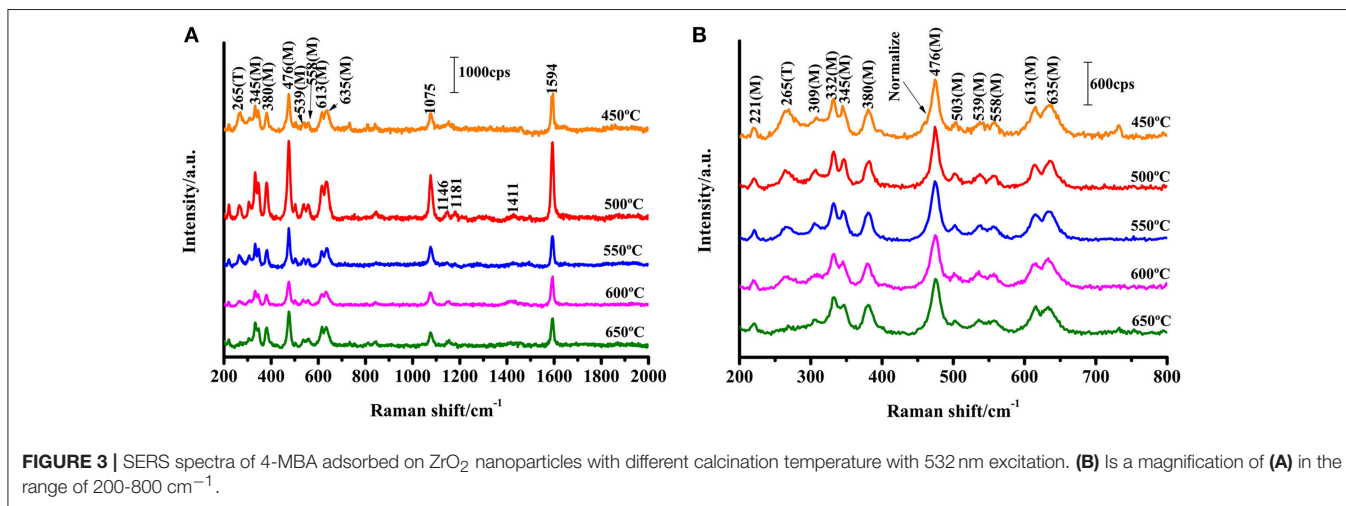

FIGURE 3 | SERS spectra of 4-MBA adsorbed on ZrO$_2$ nanoparticles with different calcination temperature with 532 nm excitation. (B) Is a magnification of (A) in the range of 200–800 cm^{-1}.

calcination temperature increases, the crystallinity also increases, resulting in a decrease in the surface defect content of the ZrO$_2$ nanoparticles (**Figure 2A**). This is also the reason for the decrease in CT effects of the ZrO$_2$ molecules. Therefore, it can be seen from **Figure 3** that at temperatures above 500°C, the SERS signal of zirconia decreases with increasing temperatures. This indicates that in the process of ZrO$_2$ molecular CT, the surface defects play an important role and a rich surface state favors the ZrO$_2$-to-molecule CT process.

The structural characteristics of the ZrO$_2$ nanostructures are analyzed by TEM techniques, as shown in **Figure S2**. Based on the results, the crystalline sizes of all of the nanoparticles are ≈10 nm in diameter, which is similar to the results obtained from the XRD patterns through calculation with the Scherrer equation. The results indicate that the size of the ZrO$_2$ nanoparticles increases with increasing calcination temperature. This indicates that the calcination temperature has a significant effect on the size of the nanoparticles. The optical properties of the ZrO$_2$ nanoparticles were further analyzed by means of UV-Vis spectra.

Calculation of the Surface Enhancement Factor (EF)

The surface enhancement factor (EF) was calculated for the 4-MBA adsorbed on ZrO$_2$ nanoparticles at an excitation of 532 nm. The assignment of each of the strong peaks in the Raman spectrum is listed in **Table S1**. The ν (C-C) ring breathing mode (∼1,594 cm^{-1}) was selected to calculate the EF of ZrO$_2$ nanoparticles. The EF calculation formula is shown in Equation (3):

$$EF = \frac{I_{surf} N_{Bulk}}{I_{Bulk} N_{Surf}} \tag{3}$$

where I represents the corresponding intensity of the selected peak, and N represents the number of molecules observed by the laser spot; N_{Bulk} is the number of bulk 4-MBA molecules under laser irradiation, N_{Surf} is the number of 4-MBA molecules involved in the surface modification of ZrO$_2$, I_{Surf} is the intensity of a vibrational mode in the SERS, and I_{Bulk} is the intensity in the conventional Raman spectra of the same mode. From the area of

the laser spot ($\sim$1.3 μm^2) and the focus penetration depth of the laser ($\sim$10 μm), the volume of the solid sample can be calculated. Based on the density (1.5 g·cm^{-3}) and volume of 4-MBA, N_{Bulk} was calculated to be 7.61 $\times$ 10^{10}. Assuming that a single layer of ZrO$_2$ nanoparticles are uniformly covered with a square centimeter of sediment, the number density is estimated to be 9.07 $\times$ 10^{11} particles/cm^2 based on the XRD (according to the XRD results, the average diameter of the zirconia nanoparticles was 10.5 nm), as shown in **Figure 2A**. Using the laser spot size and the boundary density of the adsorbing molecules on the surface of the nanoparticles ($\sim$0.5 nmol/cm^2), N_{Surf} can be calculated as 6.15 $\times$ 10^6. From the observed spectra, the ratio of intensities I$_{Surf}$/I$_{Bulk}$ = 1765.42/5051.69 = 0.349 can be obtained. Substituting the obtained values for these variables into Equation 3, the EF value is calculated as 4.32 $\times$ 10^3.

An enhancement (by a factor $\sim$3) of the Bg and Ag ZrO$_2$ phonon modes at 330 and 475 cm^{-1}, respectively, was also observed. This enhancement is similar to the enhancement mechanism for the normal mode of the molecule. The results show that an EF of more than 10^3 is achieved for 4-MBA on ZrO$_2$ nanoparticles. It has not previously been reported that SERS signals are observed on the surface of ZrO$_2$, but the results are similar to the EF for other semiconductor nanoparticles that have been reported previously.

CT Mechanism
a1 and b2 Modes of 4-MBA

The SERS signal of a near-monolayer of 4-MBA adsorbed on the surface of ZrO$_2$ nanoparticles was observed (the excess of 4-MBA on the surface was washed away with a solvent). **Figure 4** shows the Raman spectra for the bulk 4-MBA and a solution dissolved in ethanol (0.1 mol/L), as well as the enhanced Raman spectrum of 4-MBA on a ZrO$_2$ substrate. The only difference between the conventional Raman spectroscopy and SERS samples is the amount of 4-MBA molecules: in the former, a large number of pure 4-MBA molecules are present, while the latter utilizes a monolayer of 4-MBA molecules present only on the ZrO$_2$ substrate. All of the other test conditions and procedures are the same. A distinct 4-MBA signal was observed on the ZrO$_2$ substrate with clear Raman peaks at 1075, 1146, 1181, and 1594 cm^{-1}. However, because SERS modifies the surface selection rules, there is a significant difference in the relative intensities of the peaks observed for the 4-MBA molecule in the Raman and SERS spectra. The bulk 4-MBA spectrum is mainly dominated by the fully symmetric a1 vibration mode, while the SERS spectrum for 4-MBA exhibits a strong contribution of the asymmetric b2 mode (1146 cm^{-1}).

The Raman peak at 1075 cm^{-1} is attributed to aromatic ring vibration with a C-S stretching mode (ν12a, a1), while at approximately 1,594 cm^{-1} the Raman peak is assigned to the aromatic ring breathing mode (ν8a, b2). As shown in **Figure 4**, the Raman spectrum for 4-MBA adsorbed on the surface of zirconia nanoparticles was strongly enhanced compared to the conventional Raman spectrum for 4-MBA, and the Raman shift was significantly different from that of the bulk Raman spectrum. The spectrum of the 4-MBA adsorbed on the surface of zirconia nanoparticles exhibits a weak peak at 1146 cm^{-1} (ν15, b2) in the
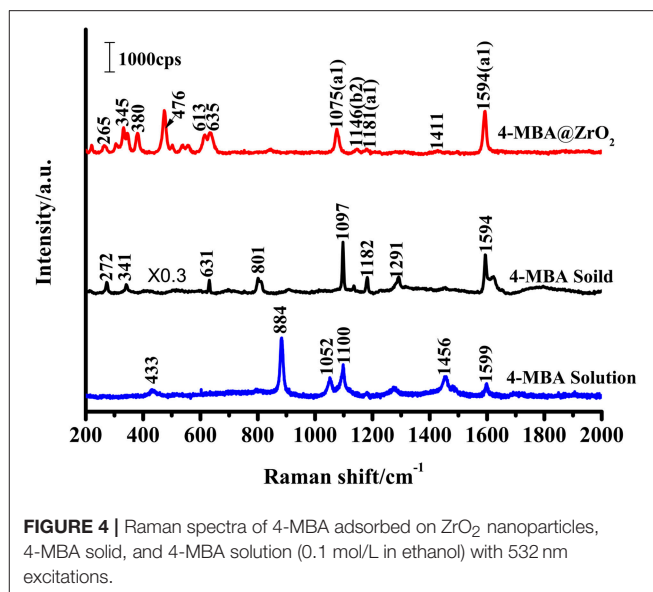

FIGURE 4 | Raman spectra of 4-MBA adsorbed on ZrO$_2$ nanoparticles, 4-MBA solid, and 4-MBA solution (0.1 mol/L in ethanol) with 532 nm excitations.

SERS spectrum (attributed to the C-H deformation vibrational mode), which is generally considered to be due to the Herzberg-Teller contribution that produces enhanced CT effects. The SERS spectrum of 4-MBA on the surface of ZrO$_2$ is almost identical to that observed on the surface of ZrO$_2$ and TiO$_2$ in the literature. We also calculated the value of P$_{CT}$, which was calculated through the expression which was defined as "P$_{CT}$ = R/(1 + R)" for the degree of charge transfer(R = I$_{b2}$/I$_{a1}$). As shown in **Figure S4**, the P$_{CT}$ of 4-MBA is near 0.5 at the excitation wavelengths of 532, 633, and 785 nm. It was observed that the degree of charge transfer increases with the increase of laser energy.

Direction of CT Effects

There are two main ways to explain the enhancement mechanism of the SERS effect: chemical mechanisms (CT) and electromagnetic mechanisms (EM). Chemical enhancement (CE) is a resonance-like Raman process. It is generated by chemical adsorption interactions between the substrate and the adsorbed molecules and photoinduced charge transfer, resulting in an increase in the polarizability and an increase in the distribution number of the adsorbed molecules in the excited state. The electromagnetic mechanisms (EM) is caused by an increase in the local electric field induced by the laser on the surface of the nanoparticles (Kadkhodazadeh et al., 2014; Mogensen and Kneipp, 2014). According to the literature, for most semiconductor materials, the surface plasmon resonance frequency is in the infrared region, away from the excitation wavelength (532 nm) used to obtain the SERS phenomenon in this study (Wang et al., 2009; Xue et al., 2012). Therefore, the SERS enhancement of ZrO$_2$ in this work does not include EM contributions, but mainly contributes to CE contributions. In **Figure 4**, the SERS spectrum of 4-MBA exhibit a non-totally symmetric b2 mode at 1146 cm^{-1}. As the CT mechanism is a resonance Raman-like process, the charge transfers occurred between the ZrO$_2$ nanocrystals and 4-MBA molecules. When

the organic molecules and semiconductor are in contact with each other, a reasonable charge distribution will exist around the interface within a very short time. A new electronic state then forms at the interface.

To determine the direction of charge transfer in the 4-MBA–ZrO$_2$ complex, Gaussian 09 was used to calculate the highest occupied molecular orbital (HOMO) and lowest unoccupied molecular orbital (LUMO) of 4-MBA molecules adsorbed on ZrO$_2$ nanoparticles, as shown in **Figure 5A**. In the 4-MBA-modified ZrO$_2$ system, the HOMO and LUMO for the 4-MBA occur at −6.75 and −1.33 eV, respectively. Thus, the CT between ZrO$_2$ and the adsorbed 4-MBA molecule may occur as shown in **Figure 5B**. In these experiments, when irradiated under a 532 nm (ca. 2.33 eV) laser, the excited electrons of the ZrO$_2$ conduction band (CB) migrate to the LUMO of the adsorbed molecules. This is a reasonable CT model to explain the SERS of ZrO$_2$ modified by 4-MBA.

Zhao et al. reported the use of UV-Vis diffuse reflectance spectroscopy (DRS; **Figure S5**) (Zhang X. et al., 2015) and ultraviolet photoelectron spectroscopy (UPS; **Figure S6**) to calculate the HOMO and LUMO of the substrate and probe molecules. This can be calculated with Equation 4:

$$W = h\nu - \Delta E \qquad (4)$$

The value of hν is 21.22 eV, and thus the valence band (VB) of ZrO$_2$ is calculated to occur at −5.19 eV. The band gap of ZrO$_2$ is

4.95 eV, and the CB of ZrO$_2$ is situated at −1.97 eV. As shown in **Figure 5B**, in the ZrO$_2$ system modified by 4-MBA, the HOMO of the 4-MBA is at −6.24 eV and the LUMO is at −1.68 eV. Therefore, considering the relative band structure of the ZrO$_2$ system with 4-MBA, the CT direction between the ZrO$_2$ and 4-MBA determined by the theoretical calculations and UPS results is consistent, i.e., the CT occurs from the zirconium dioxide to the 4-MBA molecules.

SERS Spectra of the ZrO$_2$ Surface Modified by 4-MBA, 4-MPY, and PATP

To illuminate that the enhancement mechanism of a ZrO$_2$ surface modified by 4-MBA is the CT mechanism, the following experiment was performed. The surface of ZrO$_2$ nanoparticles were modified with different thiophenol-related molecules (4-MPY and PATP), as shown in **Figure 6A**. In addition, these thiophenol-based molecules possess functional groups on the benzene ring, such as C-COOH, N, or C-NH$_2$. The electron attracting ability of these functional groups on the benzene ring occurs in the order of C-COOH (4-MBA) > N (4-MPY) > C-NH$_2$ (PATP). **Figure 6A** shows the SERS spectra for 4-MBA, 4-MPY, and PATP adsorbed on ZrO$_2$ nanoparticles. The results clearly show that the intensities decrease in the order of 4-MBA > 4-MPY > PATP. This is in agreement with the previous estimations.

As the probe molecules have almost the same Raman cross-sections, the experimental results described above are not due
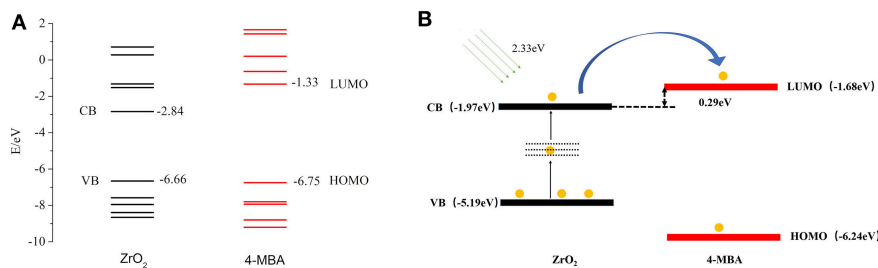

FIGURE 5 | (A) The molecular orbital illustrations of the 4-MBA molecule and ZrO$_2$ nanoparticles from calculations by Gaussian 09. **(B)** The schematic energy-level diagram at a ZrO$_2$/4-MBA molecule interfaces, and also the position of the HOMO and the LUMO of 4-MBA and the position of CB and VB of ZrO$_2$ nanoparticles.
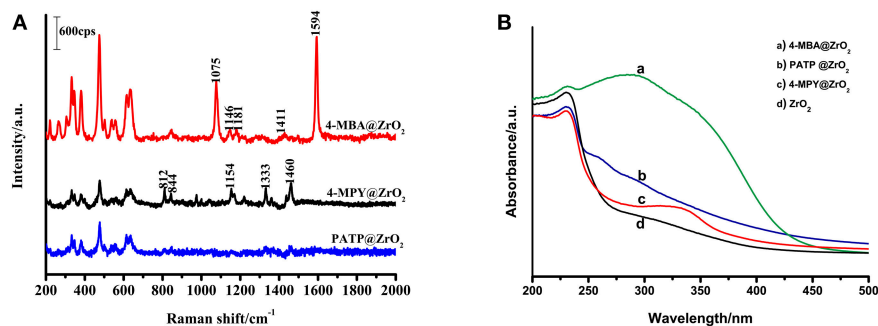

FIGURE 6 | (A) SERS spectra of 4-MBA, PATP, 4-MPY adsorbed on ZrO$_2$ nanoparticles; **(B)** UV-vis spectra of ZrO$_2$ nanoparticles and 4-MBA, PATP, 4-MPY adsorbed on ZrO$_2$ nanoparticles.

to different Raman cross-sections of the molecules. The SERS spectra effect is consistent with the ability of the mercapto-pair to attract electrons. These results indicate a correlation between the SERS signal and the ZrO$_2$-to-molecula CT. This suggests that for ZrO$_2$ nanoparticles surface-modified by other molecules, the primary enhancement mechanism is the CT mechanism. The stronger the electron-withdrawing groups in the molecules bonded on the surface of ZrO$_2$, the greater the ability of ZrO$_2$ for molecular CT will be, and a stronger SERS signal on the ZrO$_2$ will be observed.

Comparisons of the optical properties of ZrO$_2$ nanoparticles modified by molecules with those of pure ZrO$_2$ were carried out by using UV-Vis spectroscopy (**Figure 6B**). It is clear that the adsorption of organic molecules has a significant influence on the absorption spectrum of ZrO$_2$. It was observed that the typical ZrO$_2$ direct band gap adsorbs organic molecules with different degrees of narrowing and widening.

Figure S5 shows the spectra of ZrO$_2$ nanoparticles surface-modified by 4-MBA, 4-MPY, and PATP, as well as pure ZrO$_2$ nanoparticles monitored with room temperature UV-vis DRS. Using the Kubelka–Munk function, the bandgap energy of the pure ZrO$_2$ and molecule-modified ZrO$_2$ were calculated based on the photon energy $[(\alpha E)^2]$ function. The resulting band energy is 4.95 eV (250 nm) for the pure ZrO$_2$ nanoparticles, 3.22 eV (385 nm) for the 4-MBA-modified ZrO$_2$, 4.88 eV (254 nm) for the 4-MPY-modified ZrO$_2$, and 4.91 eV (253 nm) for the PATP-modified ZrO$_2$. The interaction between the adsorbed molecules and the ZrO$_2$ nanoparticle substrate resulted in these shifts. The transformation may be due to the interaction of the nanoparticles with probe molecules. The observed shift shows that the bandgap of the 4-MBA–ZrO$_2$ system has a lower optical transition energy than that of pure ZrO$_2$ due to the CT transition. The 4-MBA–ZrO$_2$ system has the lowest optical transition energy, which explains why the ZrO$_2$ modified by 4-MBA has the strongest SERS effect.

CONCLUSION

This study first observed that the SERS spectrum can be obtained on the surface of ZrO$_2$. The results show that the SERS spectrum

of 4-MBA on ZrO$_2$ is mainly due to the contribution of the CT mechanism, and the intrinsic properties of the adsorbed molecules and the surface properties of the semiconductor have a significant effect on SERS. The plentiful surface state of the ZrO$_2$ active substrate is beneficial for the occurrence of CT resonance between molecules and the ZrO$_2$ to produce a SERS effect. The results show that the ZrO$_2$ nanoparticles prepared through the sol-gel method at a calcination temperature of 500°C exhibit the strongest SERS effect on the surface-adsorbed probe molecules. This study demonstrates for the first time that ZrO$_2$ can be used as a Raman enhancement substrate material, breaking through the limitations of the precious metal substrates used in traditional SERS technology, and further broadening the application of semiconductor oxides as substrate materials for SERS detection. Also, the SERS study on the size effect of nano-sized ZrO$_2$ is expected to promote the better performance of nano-ceramic materials to enable the emergence of new properties and functions.

AUTHOR CONTRIBUTIONS

XiuS designed the experiment. PJ conducted experiments and characterization. ZW funded some of the subject experiments. XiaS assisted in the theoretical simulation. YZ and YL participated in the discussion. PJ, XiuS, and ZM wrote the manuscript together.

FUNDING

SUPPLEMENTARY MATERIAL

The Supplementary Material for this article can be found online at: https://www.frontiersin.org/articles/10.3389/fchem.2019.00245/full#supplementary-material

REFERENCES

Alessandri, I., and Lombardi, J. R. (2016). Enhanced raman scattering with dielectrics. *Chem. Rev.* 116, 14921–14981. doi: 10.1021/acs.chemrev.6b00365

Becker, J., Hald, P., Bremholm, M., Pedersen, J. S., Chevallier, J., Iversen, S. B., et al. (2008). Critical size of crystalline ZrO2 nanoparticles synthesized in near- and supercritical water and supercritical isopropyl alcohol. *ACSnano* 2, 1058–1068. doi: 10.1021/nn7002426

Carlone, C. (1992). Raman spectrum of zirconia-hafnia mixed crystals. *Phys. Rev. B* 45, 2079–2084. doi: 10.1103/physrevb.45.2079

Chang, S., and Doong, R. (2007). Interband transitions in Sol–Gel-Derived ZrO2 films under different calcination conditions. *Chem. Mater.* 19, 4804–4810. doi: 10.1021/cm070606n

De Aza, A. H., Chevalier, J., Fantozzi, G., Schehl, M., and Torrecillas, R. (2002). Crack growth resistance of alumina, zirconia andzirconia toughened alumina ceramics for joint prostheses. *Biomaterials* 23, 937–945. doi: 10.1016/S0142-9612(01)00206-X

Duan, H., Unno, M., Yamada, Y., and Sato, S. (2017). Adsorptive interaction between 1,5-pentanediol and Mgo-Modified ZrO2 catalyst in the vapor-phase dehydration to produce 4-Penten-1-Ol. *Appl. Cataly. A Gen.* 546, 96–102. doi: 10.1016/j.apcata.2017.07.048

Fu, X., Wang, Y., Liu, Y., Liu, H., Fu, L., Wen, J., et al. (2019). A graphene oxide/gold nanoparticle-based amplification method for SERS immunoassay of cardiac troponin I. *Analyst* 144, 1582–1589. doi: 10.1039/c8an02022a

Gan, X., Yu, Z., Yuan, K., Xu, C., Wang, X., Zhu, L., et al. (2017). Preparation of a CeO2-nanoparticle thermal radiation shield coating on ZrO2 fibers Via a hydrothermal method. *Ceram. Int.* 43, 14183–14191. doi: 10.1016/j.ceramint.2017.07.161

Han, X. X., Ji, W., Zhao, B., and Ozaki, Y. (2017). Semiconductor-enhanced raman scattering: active nanomaterials and applications. *Nanoscale* 9, 4847–4861. doi: 10.1039/c6nr08693d

Heuer, A. H., Claussen, N., , Kriven, W. M., and Ruhle, M. (1982). Stability of tetragonal ZrO2 particles in ceramic matrices. *J. Am. Ceram. Soc.* 65, 643–650. doi: 10.1111/j.1151-2916.1982.tb09946.x

Huang, Y. F., Zhang, M., Zhao, L. B., Feng, J. M., Wu, D. Y., Ren, B., et al. (2014). Activation of oxygen on gold and silver nanoparticles assisted by surface plasmon resonances. *Angew. Chem. Int. Edn.* 53, 2353–2357. doi: 10.1002/ange.201310097

Jiang, L., You, T., Yin, P., Shang, Y., Zhang, D., Guo, L., et al. (2013). Surface-enhanced raman scattering spectra of adsorbates on Cu(2)O nanospheres: charge-transfer and electromagnetic enhancement. *Nanoscale* 5, 2784–2789. doi: 10.1039/c3nr33502j

Kadkhodazadeh, S., de Lasson, J. R., Beleggia, M., Kneipp, H., Wagner, J. B., and Kneipp, K. (2014). Scaling of the surface plasmon resonance in gold and silver dimers probed by eels. *J. Phys. Chem. C.* 118, 5478–5485. doi: 10.1021/jp500288s

Kralik, B., Chang, E. K., and Louie, S. G. (1998). Structural properties and quasiparticle band structure of zirconia. *Phys. Rev. B.* 57:7027. doi: 10.1103/physrevb.57.7027

Li, J., Chen, L., Lou, T., and Wang, Y. (2011). Highly sensitive SERS detection of As3+ ions in aqueous media using glutathione functionalized silver nanoparticles. *ACS Appl. Mater. Interfaces* 3, 3936–3941. doi: 10.1021/am200810x

Li, X., Xu, Y., Mao, X., Zhu, Q., Xie, J., Feng, M., et al. (2017). Investigation of optical, mechanical, and thermal properties of ZrO_2-Doped Y_2O_3 transparent ceramics fabricated by Hip. *Ceram. Int.* 44, 1362–1369. doi: 10.1016/j.ceramint.2017.08.204

Lombardi, J. R., and Birke, R. L. (2014). Theory of surface-enhanced raman scattering in semiconductors. *J. Phys. Chem. C* 118, 11120–11130. doi: 10.1021/jp5020675

Long, D., Niu, M., Tan, L., Fu, C., Ren, X., Xu, K., et al. (2017). Ball-in-Ball ZrO_2 nanostructure for simultaneous Ct imaging and highly efficient synergic microwave ablation and tri-stimuli-responsive chemotherapy of tumors. *Nanoscale* 9, 8834–8847. doi: 10.1039/c7nr02511d

Mogensen, K. B., and Kneipp, K. (2014). Size-dependent shifts of plasmon resonance in silver nanoparticle films using controlled dissolution: monitoring the onset of surface screening effects. *J. Phys. Chem. C* 118, 28075–28083. doi: 10.1021/jp505632n

Navio, J., Hidalgo, M., Colon, G., Botta, S., and Litter, M. (2001). Preparation and physicochemical properties of ZrO_2 and Fe/ZrO_2 prepared by a Sol– Gel Technique. *Langmuir* 17, 202–210. doi: 10.1021/la000897d

Scott, B. L., and Carron, K. T. (2016). Dynamic raman scattering studies of coated gold nanoparticles: 4-mercaptopyridine, 4-mercaptophenol, and benzenethiol. *J. Phys. Chem. C* 120, 20905–20913. doi: 10.1021/acs.jpcc.6b02617

Shen, W., Lin, X., Jiang, C., Li, C., Lin, H., Huang, J., et al. (2015). Reliable quantitative sers analysis facilitated by core–shell nanoparticles with embedded internal standards. *Angew. Chem. Int. Edn.* 54, 7308–7312. doi: 10.1002/ange.201502171

Shiohara, A., Wang, Y., and Liz-Marzán, L. M. (2014). Recent approaches toward creation of hot spots for sers detection. *J. Photochem. Photobiol. C.* 21, 2–25. doi: 10.1016/j.jphotochemrev.2014.09.00

Sun, Z., Zhao, B., and Lombardi, J. R. (2007). ZnO nanoparticle size-dependent excitation of surface raman signal from adsorbed molecules: observation of a charge-transfer resonance. *Appl. Phys. Lett.* 91:221106. doi: 10.1063/1.2817529

Wang, C., Guan, Q., Wu, F., and Wang, H. (2019). A novel Mgo doped Zr0.92y0.08O2-Î'(8ysz) with NaCl/KCl composite electrolyte for intermediate temperature fuel cells. *Ceram. Int.* 45, 1605–1608. doi: 10.1016/j.ceramint.2018.10.035

Wang, Y., and Chen, L. (2011). Quantum dots, lighting up the research and development of nanomedicine. *Nanomedicine* 7, 385–402. doi: 10.1016/j.nano.2010.12.006

Wang, Y., Ji, W., Sui, H., Kitahama, Y., Ruan, W., Ozaki, Y., et al. (2014). Exploring the effect of intermolecular H-bonding: a study on charge-transfer contribution to surface-enhanced raman scattering of P-mercaptobenzoic acid. *J. Phys. Chem. C* 118, 10191–10197. doi: 10.1021/jp5025284

Wang, Y., Ruan, W., Zhang, J., Yang, B., Xu, W., Zhao, B., et al. (2009). Direct observation of surface-enhanced Raman scattering in ZnO nanocrystals. *J. Raman Spectrosc.* 40, 1072–1077. doi: 10.1002/jrs.2241

Wang, Y., Sun, Z., Wang, Y., Hu, H., Zhao, B., Xu, W., et al. (2007). Surface-enhanced raman scattering on mercaptopyridine-capped CdS microclusters. *Spectrochim. Acta. Part A Mole. Biomol. Spectrosc.* 66, 1199–1203. doi: 10.1016/j.saa.2006.06.008

Wang, Y., Wang, Y., Wang, W., Sun, K., and Chen, L. (2016). Reporter-embedded SERS tags from gold nanorod seeds: selective immobilization of reporter molecules at the tip of nanorods. *ACS Appl. Mater. Interfaces* 8, 28105–28115. doi: 10.1021/acsami.6b04216

Wang, Y., Yan, B., and Chen, L. (2013). SERS tags: novel optical nanoprobes for bioanalysis. *Chem. Rev.* 113, 1391–1428. doi: 10.1021/cr300120g

Xu, S., Xu, Y., Liu, Y., Fang, M., Wu, X., Min, X., et al. (2017). Fabrication and abrasive wear behavior of ZrO_2-SiC-Al_2O_3 ceramic. *Ceram. Int.* 43, 15060–15067. doi: 10.1016/j.ceramint.2017.08.032

Xue, X., Ji, W., Mao, Z., Mao, H., Wang, Y., Wang, X., et al. (2012). Raman investigation of nanosized TiO_2: effect of crystallite size and quantum confinement. *J. Phys. Chem. C* 116, 8792–8797. doi: 10.1021/jp2122196

Yang, L., Jiang, X., Ruan, W., Zhao, B., Xu, W., and Lombardi, J. R. (2008). Observation of enhanced raman scattering for molecules adsorbed on Tio_2 nanoparticles: charge-transfer contribution. *J. Phys. Chem. C* 112, 20095–20098. doi: 10.1021/jp8074145

Yin, P. G., Jiang, L., You, T. T., Zhou, W., Li, L., and Guo, L. (2010). Surface-enhanced Raman spectroscopy with self-assembled cobalt nanoparticle chains: comparison of theory and experiment. *Phys. Chem.* 12, 10781–10785. doi: 10.1039/c002662j

Zhang, L., Huang, Z., Pan, W., and Krell, A. (2015). High transparency Nd: Y_2O_3ceramics prepared with La_2O_3 and ZrO_2 additives. *J. Am. Ceram. Soc.* 98, 824–828. doi: 10.1111/jace.13354

Zhang, X., Yu, Z., Ji, W., Sui, H., Cong, Q., Wang, X., et al. (2015). Charge-transfer effect on Surface-Enhanced Raman Scattering (SERS) in an ordered Ag Nps/4-mercaptobenzoic Acid/TiO_2 system. *J. Phys. Chem. C* 119, 22439–22444. doi: 10.1021/acs.jpcc.5b06001

Zhao, L. B., Zhang, M., Huang, Y. F., Williams, C. T., Wu, D. Y., Ren, B., et al. (2014). Theoretical study of plasmon-enhanced surface catalytic coupling reactions of aromatic amines and nitro compounds. *J. Phys. Chem. Lett.* 5, 1259–1266. doi: 10.1021/jz5003346

Zhao, X., and Vanderbilt, D. (2002). Phonons and lattice dielectric properties of zirconia. *Phys. Rev. B.* 65:075105. doi: 10.1103/PhysRevB.65.075105

Zheng, H., Liu, K., Cao, H., and Zhang, X. (2009). L-Lysine-assisted synthesis of ZrO_2 nanocrystals and their application in photocatalysis. *J. Phys. Chem. C* 113, 18259–18263. doi: 10.1021/jp9057324

Zhou, L., Xu, J., Li, X., and Wang, F. (2006). Metal oxide nanoparticles from inorganic sources via a simple and general method. *Mater. Chem. Phys.* 97, 137–142. doi: 10.1016/j.matchemphys.2005.07.062